Progress In Electromagnetics Research, Vol. 144, 23–31, 2014

Classification of Targets Improved by Fusion of the Range Profile and the Inverse Synthetic Aperture Radar Image

In-O Choi[1], Joo-Ho Jung[2], Si-Ho Kim[3], Kyung-Tae Kim[2], and Sang-Hong Park[1, *]

Abstract—The range profile (RP) and the inverse synthetic aperture radar (ISAR) image are the useful radar signatures for classifying unknown targets because they can be used regardless of day-night and weather conditions. Since classification that uses RP and ISAR is heavily dependent on flight conditions, however, much more study is required on this topic. This paper proposes an efficient method of classifying targets by using a classifier-level fusion of RP and ISAR as well as a scenario-based construction method of the training database. Simulation results using the five targets composed of point scatterers prove that the proposed method yields high classification results when the targets are flying in a variety of directions at both short and long ranges.

1. INTRODUCTION

Automatic Target Recognition (ATR) is a technique used to recognize air-to-air or land-to-air targets on real-time basis. The two representative methods for ATR are the range profile (RP) and the inverse synthetic aperture radar (ISAR) image. RP is one dimensional (1D) distribution of the radar cross section (RCS) [1–4], which is derived by compressing the wideband radar signal. ISAR is the 2D image of the target derived by coherently processing RPs and conducting the translational motion compensation [5, 6]. Because of the limited memory space and the classification time, ATR using RP and ISAR is conducted by using the scenario-based construction method in which the training database is constructed based on the flight scenario, and the classification is performed by matching the training data corresponding to the flight scenario [7, 8].

However, the classification using the two methods is heavily dependent on flight conditions [9]. When the target is flying in the direction of the radar line of sight (LOS), the classification ratio (P_c) derived using ISAR is degraded significantly because the image plane formed by the vertical angular variation causes scatters to be distributed in a narrow region on the image. On the other hand, when the target is flying in the vertical direction of LOS, P_c by RP is degraded due to the dominant peak that makes each target look similar. Therefore, a correct classification method that can be used for all flight directions is required.

In this paper, we propose an efficient classification method that yields high P_cs regardless of the flight directions by fusing RP and ISAR on classifier-level. In simulations assuming the flight at both short and long ranges using the five aircraft models composed of scatterers, the proposed method was very robust to the flight direction, signal-to-noise ratio (SNR) and the size of the training database, yielding P_cs $\geq 98\%$ at long ranges and P_cs $\geq 86\%$ at short ranges.

Received 22 October 2013, Accepted 11 December 2013, Scheduled 12 December 2013

* Corresponding author: Sang-Hong Park (radar@pknu.ac.kr).

[1] Department of Electronic Engineering, Pukyong National University, Busan, Korea. [2] Department of Electrical Engineering, Pohang University of Science and Technology, Pohang, Gyungbuk, Korea. [3] Agency for Defense Development, Daejeon, Korea.

2. PRINCIPLES

2.1. Signal Modeling

For maximum SNR, the matched-filter is widely used by compressing pulse-width of arbitrary-shaped signals. The matched-filtered signal is given by

$$|\chi(\tau,0)| = |g(t) \otimes h(t)| = \left| \int_{-\infty}^{\infty} g(\tau)h(t-\tau)d\tau \right| = \left| \int_{-\infty}^{\infty} g(\tau)s^*(t-\tau)d\tau \right|, \tag{1}$$

where $g(t)$ is a received signal at time t, and $h(t)$ is an impulse response whose form equals to the conjugate of the transmitted signal $s(t)$. To reduce the computation time, this procedure can be conducted in the frequency domain, and then we assume the monostatic chirp radar signal for high range resolution of $\Delta r = c/2B$ (c = Speed of light, B = bandwidth) [10]. The transmitted chirp signal $s(t)$ is

$$s(t) = A_0 e^{j2\pi\left(f_0 t + \frac{B}{2\tau}t^2\right)} \times rect\left[\frac{t}{\tau}\right], \tag{2}$$

where A_0 is the amplitude, f_0 the start frequency, B the bandwidth, τ the pulse duration, and $rect$ a function whose value is 1 for $t - \tau/2 \leq t \leq t + \tau/2$ and 0 otherwise. We assume that the target is composed of K point scatterers and far-field. Then the received chirp signal $g(t)$ at aspect angle θ is

$$g(\theta,t) = \sum_{k=1}^{K} A_k e^{j2\pi\left[f_0(t-d_{k,\theta}) + \frac{B}{2\tau}(t-d_{k,\theta})^2\right]} \times rect\left[\frac{t-d_{k,\theta}}{\tau}\right], \tag{3}$$

where A_k is the amplitude of scattering center k, and $d_{k,\theta}$ is the time delay between the radar and scattering center k. Finally, the high resolution RP with corresponding backscattered field amplitudes comes as a result of matched-filtering [10].

For ISAR imaging, it is required to collect the angular variation $\Delta\theta$ that yields the same cross-range resolution $\Delta r_c = \lambda/2\Delta\theta$ (λ = wavelength) as the range resolution δr. Then, we get the data through translation motion compensation such as range-Doppler algorithm [11, 12] and obtain ISAR images by applying the azimuth compression to each bin of the range profiles using the Fourier transform.

2.2. Feature and Classifier for RP

This paper uses the feature vector of multi-aspect RPs [13]. This method provides a classification more advanced than the single-aspect method in terms of the limited band, and it is based on the central moment (CM) that is invariant to translation of RPs. For CM, the RP is regarded as a probability density function by normalizing by the sum of the total values and the CM of the order p is given by

$$\mu_p = \sum_{n=0}^{N_r-1} (n-\eta_r)^p \left[\frac{\bar{p}(n)}{\sum_{i=0}^{N_r-1} \bar{p}(i)}\right], \tag{4}$$

where η_r is the mean value, $\bar{p}(n)$ the amplitude of the component n in RP normalized, p the order of the CM, and N_r the number of range bins in RP. Then, the principal component analysis (PCA) is used to remove the redundancy in the vector and reduce the necessary feature space dimension [14]. For the multi-aspect classification using RPs obtained at various aspect angles, (4) is changed as follows:

$$\mu_{j,p} = \sum_{n=0}^{N_{j,r}-1} (n-\eta_{j,r})^p \left[\frac{\bar{p}_j(n)}{\sum_{i=0}^{N_{j,r}-1} \bar{p}_j(i)}\right], \quad j = 0, 1, \ldots, N_M \tag{5}$$

where $\eta_{j,r}$, $\bar{p}_j(n)$, $N_{j,r}$ are the CM parameters of aspect angle j, and N_M is the number of aspect angles. For the classifier, we use the nearest neighbor classifier (NNC) that uses a simple Euclidean distance between two feature vectors as follows [15]:

$$d(x_1, x_2) = |\bar{x}_1 - \bar{x}_2| . \tag{6}$$

The minimum distance value yields the one that the unknown target belongs to. However, because several RPs are used to obtain the ISAR image, the multi-aspect classification method is used to improve the classification result, which is conducted on the basis of the following rule:

$$i^* = \max_k N_k, \tag{7}$$

where N_k is the number of kth class decisions [13]. The target having the largest N_k is the one that an unknown target belongs to.

2.3. Polar Mapping Classifier for ISAR

To classify ISAR image, we use the polar mapping classifier (PMC) that is invariant to the variation of the scale and the translation of the ISAR image [16]. With the use of polar mapping, we can obtain the resampled polar image as follows:

$$(x_k, y_k) = (x_c, y_c) + (r_m \cos\theta_n, r_m \sin\theta_n). \tag{8}$$

r_m is the sampling point of the order m in r direction, θ_n the order n in θ direction, and (x_c, y_c) the center position of the polar mapping (Fig. 1). In classification, we use a projection of the polar mapped image onto the r-axis, a projection onto θ-axis. Then, targets are coarsely sifted through similarity of targets in the training database using the correlation coefficients of r-projected images, and fine-sifted by seeking the maximum cross-correlation of θ-projected images (see [16] for the detailed procedure). To reduce the computation time, the maximum correlation was found using the relationship between Fourier transform and correlation. The maximum correlation value between two feature vectors was obtained by Fourier transforming the two vectors, element-wise multiplying one Fourier transformed vector and the conjugate of the other, inverse Fourier transforming the element-wise multiplication, and finding the maximum value.

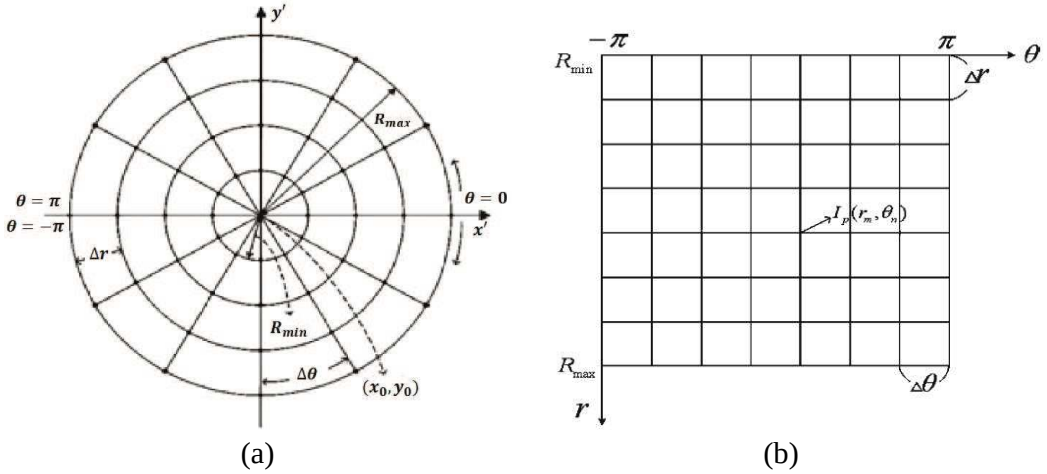

Figure 1. Principle of polar mapping [14]. (a) Polar grids. (b) Geometry of polar image.

2.4. Proposed Method to Construct the Training Database Based on the Flight Scenario

For the construction of the training database, we used the scenario-based method proposed in [7]. This method reduces the memory space and the classification time significantly by constructing the training

database based on the flight scenario (Fig. 2). The clustering-based method can further reduce the training database size [8], however, this method was not used in this paper because the whole dataset should be readjusted whenever a new target is added in the real ATR scenario. In addition, poorly clustered classes due to a large number of targets may cause performance degradation.

Assuming the flight scenario, we constructed the training space using $a_{xl} \leq x \leq a_{xu}$, $a_{yl} \leq y \leq a_{yu}$ and $a_{zl} \leq z \leq a_{zu}$. The training space was uniformly divided into $N_c \times N_c \times N_c$ grid points in each of three axes (Fig. 2(a)), and starting from each given grid point, R_0, the RPs of a target were collected using the target flying with a given constant velocity v in a direction vector $\vec{n}_d = [\sin\theta_d, -\cos\theta_d, 0]$ until the aspect angle variation $\Delta\theta = \lambda/2\Delta r_c$ that satisfies a given cross-range resolution of the ISAR image was obtained.

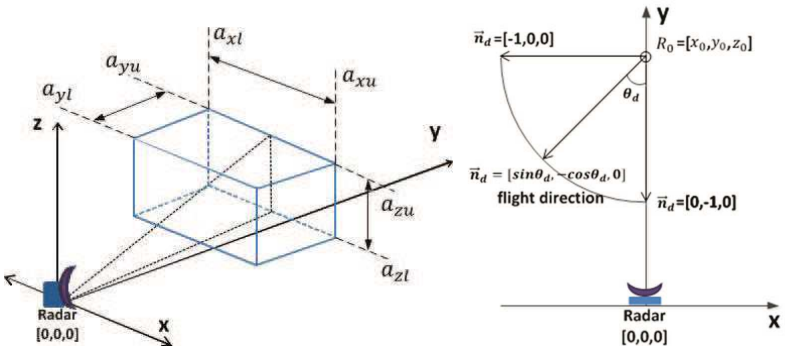

(a) (b)

Figure 2. Scenario-based construction method. (a) Example of training space. (b) Flight direction (Top view).

The test database which was constructed by the multi-aspect feature vectors compressed by PCA and polar vectors derived by 50 images of each target was stored for the classification of RP and ISAR image, respectively. For successful classification of the unknown target in all directions, θ_d was varied between 0 and 90° with a given increment $\Delta\theta_d$. Finally, the classification was conducted by comparing the training data with test data derived from the flight scenario of the test target.

2.5. Proposed Classification Method

In this paper, two classifiers mentioned in Subsections 2.2 and 2.3 were efficiently merged to improve the classification result regardless of the flight directions. In the first step, two vectors, $\vec{r}_{RP}$ and $\vec{r}_{ISAR}$, whose elements are the ranking of each target determined by classifying multi-aspect RPs and a test ISAR, are constructed as follows:

$$\vec{r}_{RP} = [i_1, i_2, \ldots, i_N], \quad \vec{r}_{ISAR} = [j_1, j_2, \ldots, j_N], \tag{9}$$

where i_n and j_n are the ranking of the target n after classification.

In the second step, a new classifier independent of the flight direction θ_d was formed by imposing the flight-direction-dependent weight on $\vec{r}_{RP}$ and $\vec{r}_{ISAR}$; larger weight was put on $\vec{r}_{RP}$ when θ_d was small and vice versa for $\vec{r}_{ISAR}$. However, because the ranking of RP and ISAR is heavily dependent on θ_d, we used two types of weight, linear and sinusoidal as follows:

$$\vec{I} = \omega_1 \left[\frac{\theta_{max} - \theta_d}{\theta_{max}} \times \vec{r}_{RP} \right] + \omega_2 \left[\frac{\theta_d}{\theta_{max}} \times \vec{r}_{ISAR} \right], \tag{10}$$

$$\vec{I}_s = \omega_1 \left[\cos\theta_d \times \vec{r}_{RP} \right] + \omega_2 \left[\sin\theta_d \times \vec{r}_{ISAR} \right], \tag{11}$$

where $\vec{I}$ and $\vec{I}_s$ are the ranking derived by linear and sinusoidal weights. ω_1 and ω_2 are additional coefficients to compensate for the deviation of classification results for various θ_ds from the linear and the sinusoidal lines.

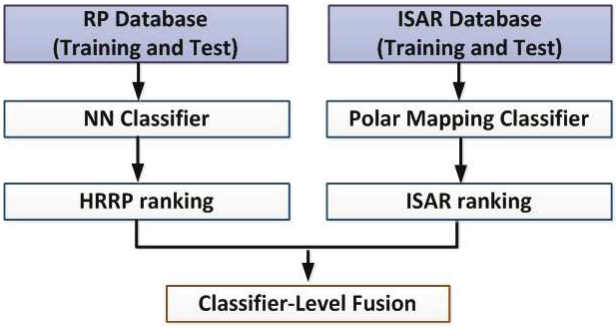

Figure 3. Classification procedure.

Table 1. Scenario parameters.

Long range scenario (Km)	Short range scenario (Km)
$-4 \leq x \leq 4$	$-4 \leq x \leq 4$
$80 \leq x \leq 120$	$8 \leq x \leq 12$
$2 \leq x \leq 10$	$2 \leq x \leq 10$

Methods based on the fuzzy system can be utilized [17], however, these were not used in this paper because the whole dataset should be readjusted by adjusting the parameter of the membership function of the fuzzy system whenever a new target is added to the existing database. The overall procedure is summarized in Fig. 3.

3. SIMULATION RESULTS

3.1. Simulation Setup

In simulations, we used five targets consisting of isotropic point scatterers which were derived by using the 3D CAD data of real aircraft; Boeing 737, F18, F14, Su35 and Rafale jets (www.3dcadbrowser.com). For the radar system, we used a monostatic chirp radar with a pulse repetition frequency = 2 kHz, center frequency = 9.15 GHz, bandwidth = 200 MHz (cross-range resolution $\Delta r_c = 0.75$ m) and the pulse width $\tau = 30\,\mu$s.

In constructing the training database, two flight scenarios, long and short ranges, were considered using the parameters specified in Table 1. The targets were flown at $v = 300$ m/s in a flight direction $\vec{n}_d = [\sin\theta_d, -\cos\theta_d, 0]$ until the variation of the aspect angle $\Delta\theta = 1.26^\circ$ corresponding to cross-range resolution was obtained, and the obtained RPs and ISAR images were stored in the training database. To study the effect of the training database size, $\Delta\theta_d$ and N_c were varied starting from 5° and 20, respectively.

For the construction of the test database, 50 images of each target and the corresponding RPs were derived by flying the target from a random position in the training space in a random direction using a random θ_d selected in a range $0 \leq \theta_d \leq 90^\circ$. For the aircraft motion, to consider the difference between the training and the test targets, v and a were selected randomly in the range of aircraft velocity and acceleration, i.e., $250 \leq v \leq 350$ m/ and $0 \leq a \leq 5\,\text{m/s}^2$. SNR was varied from 0 to 30 dB with an increment of 5 dB to study the effect of noise. In the classification of the RP, the order of PCA was set to 8.

3.2. Effect of Flight Direction

The effect of the flight direction was simulated to demonstrate the efficiency of the RP and the ISAR image. With SNR = 30 dB and $N_c = 20$, 250 test data (50 per target) were formed for a given θ_d using the random initial position, v, and a. θ_d was varied from 0° to 90° with an increment $\Delta\theta_d$.

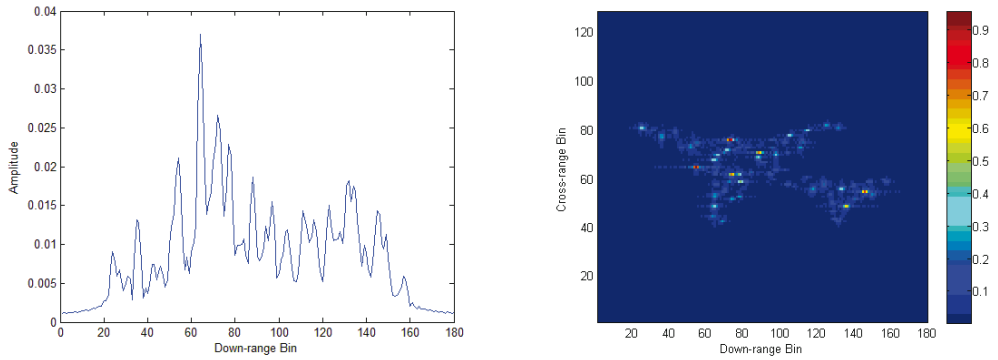

Figure 4. RP and ISAR image of Boeing 737. (a) Range profile. (b) ISAR image.

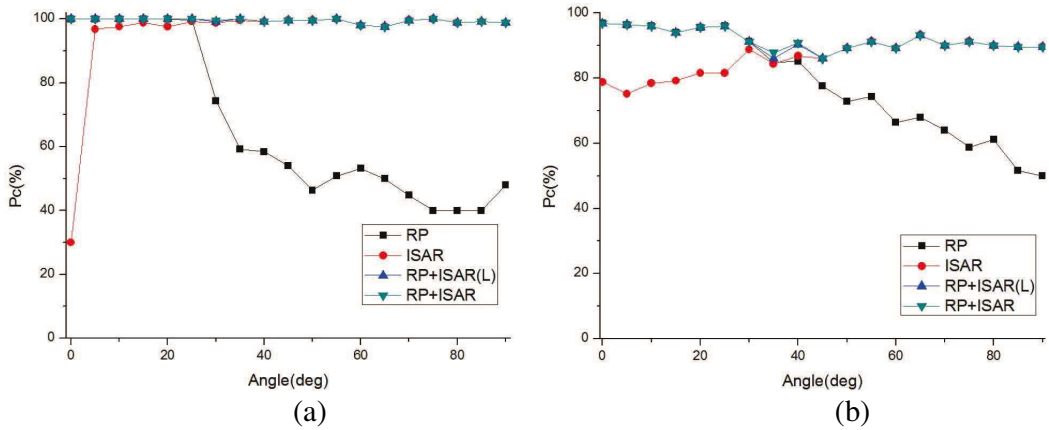

Figure 5. Classification result versus θ_d. (a) Long range. (b) Short range.

As can be seen in Fig. 4, in long range scenario, P_cs of RP at $\theta_d \geq 30°$ degraded rapidly because of the similar RPs of the targets and those of ISAR at $\theta_d \leq 5°$ were approximately equal to 30% because of the image plane formed by the vertical angular variation which made the scatterers distributed in a narrow region on the image. However, P_cs in RP + ISAR were very stable and higher than 98% for all θ_ds (Fig. 5(a)) because the proposed fusion method exploited the useful characteristics of each method for a given flight direction. In the case of the short range, P_cs obtained from RP + ISAR were lower by 5–12% because of the effect of elevation variation (Fig. 5(b)). Considering the general observation scenario conducted at a long range, the proposed method is very effective for the real flight scenario.

3.3. Effect of SNR

The influence of SNR on the classification was simulated. For each SNR, with $N_c = 20$, $\Delta\theta_d = 5°$, the aircraft flew in a random direction by selecting θ_d randomly between 0° to 90°. The proposed method was very robust to the variation of SNR in the long range scenario; P_cs higher than 98.8% were obtained for all SNR values (Fig. 6(a)). In the short range scenario, the result was lower by approximately 10% than that of the long range scenario (Fig. 6(b)). The result of RP classification was much lower than that of RP + ISAR and ISAR only because of the heavy dependency of RP on the aspect angle (see Figs. 5(a) and (b)). The effect of noise was relatively insignificant because the matched-filtering provided the maximum SNR $= 2E/N_0$, where E is the energy of the signal and $N_0/2$ is the power spectral density of the additive white Gaussian noise (see [10]). In addition, the autofocus using entropy minimization removed the noise by focusing the ISAR image and this yielded stable P_cs for all SNR values.

3.4. Effect of the Training Database Size

Because the size of the training database can be very problematic when the number of targets is large, classification must be conducted using the minimum number of training data. Therefore, we studied the effect of the training database size. As Subsection 3.3, the aircraft flew in a random direction with SNR = 30 dB, and classifications were conducted by varying $\Delta\theta_d$ and N_c. $\Delta\theta_d$ was varied between 5° and 20° with an increment of 5°, and N_c was varied between 20 and 35 with an increment of 5.

The proposed method was very robust to the reduction of the training database size (Figs. 7 and 8). For the reduction of the samples of the flight direction ($\Delta\theta_d$), the proposed method yielded $P_c s \geq 98\%$

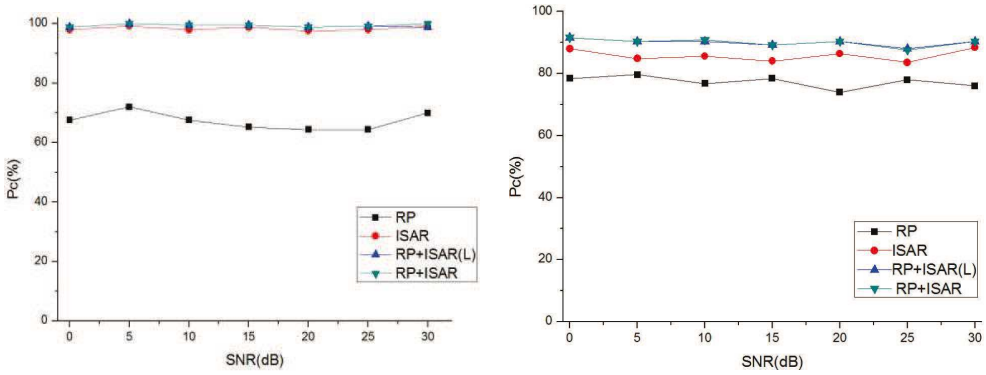

Figure 6. Classification result versus SNR. (a) Long range. (b) Short range.

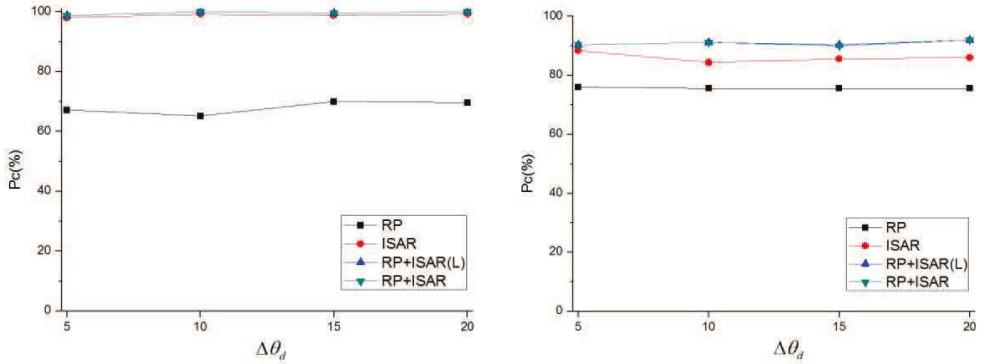

Figure 7. Classification result versus $\Delta\theta_d$. (a) Long range. (b) Short range.

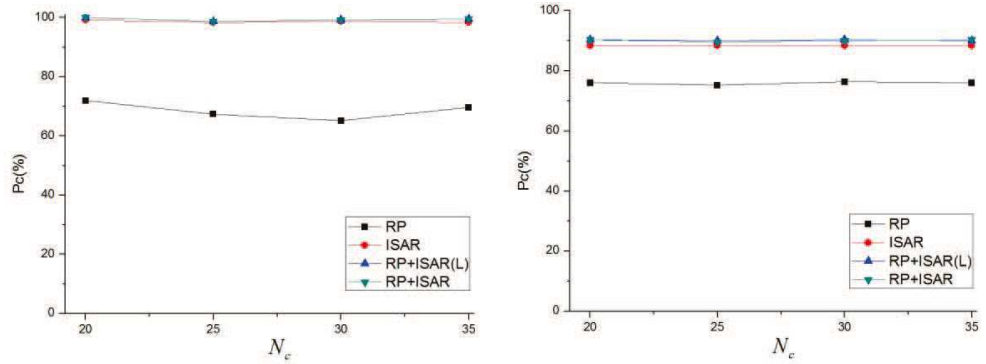

Figure 8. Classification result versus N_c. (a) Long range. (b) Short range.

in the long range observation (Fig. 7(a)) and $P_cs \geq 90\%$ in the short range observation (Fig. 7(b)). For the reduction of the grid points, P_cs were insensitive to N_c reduction; $P_cs > 98\%$ in long range (Fig. 8(a)) and $P_cs > 92\%$ (Fig. 8(b)) in short range were yielded by the proposed method. Therefore, these findings led us to conclude that the proposed method can provide a high classification result even when a very small training database is used. Because the number of targets and the flight scenario of each target can be very diverse, further study is required to determine the optimum $\Delta\theta_d$ and N_c for the efficient classification.

4. CONCLUSION

In this paper, we propose a fusion method for efficient classification of military targets. The proposed method is based on a classifier-level fusion of RP and ISAR, which is invariant to flight directions. In simulations based on flight scenario, the proposed method yielded high classification results ($P_c > 98\%$) that are insensitive to flight directions, especially when the flight scenario was in a long range. The proposed method in the long range also yielded stable classification results to SNR, the number of training data. When the target moved in a short range scenario, P_c decreased because of the effect of the elevation variation.

The simulation result, compared with the cases when only RP or ISAR is used, lead us to conclude that high classification results are yielded by RP+ISAR when the targets are flying in a variety of directions at long range. However, there can be more signatures that can be fused with RP and ISAR. One promising technique is a modulated jet engine which is a periodic Doppler modulation by the fast rotating blade of the jet engine. Currently we are focusing on the improvement of classification results on this topic using the time-frequency technique, and the improved results will be published in the open literature in the near future.

ACKNOWLEDGMENT

This research was supported by Basic Science Research Program through the National Research Foundation of Korea(NRF) funded by the Ministry of Education, Science and Technology (2012R1A1A1002047). This work was supported by the STRL (Sensor Target Recognition Laboratory) program of Defense Acquisition Program Administration and Agency for Defense Development.

REFERENCES

1. De Cos, M. E., Y. Alvarez-Lopez, and F. L. H. Andres, "On the influence of coupling AMC resonances for RCS reduction in the SHF band," *Progress In Electromagnetics Research*, Vol. 117, 103–119, 2011.
2. De Cos, M. E., Y. A. Lopez, and F. L. H. Andres, "A novel approach for RCS reduction using a combination of artificial magnetic conductors," *Progress In Electromagnetics Research*, Vol. 107, 147–159, 2010.
3. Park, H.-G., K. K. Park, H.-T. Kim, and K.-T. Kim, "Improvement of RCS prediction using modified angular division algorithm," *Progress In Electromagnetics Research*, Vol. 123, 105–121, 2012.
4. Park, H.-G., H.-T. Kim, and K.-T. Kim, "Beam tracing for fast RCS prediction of electrically large targets," *Progress In Electromagnetics Research M*, Vol. 20, 29–42, 2011.
5. Chen, C. C. and H. C. Andrews, "Target-motion-induced radar imaging," *IEEE Trans. Aerosp. Electron. Syst.*, Vol. 16, No. 1, 2–14, Jan. 1980.
6. Park, S.-H., K.-K. Park, J.-H. Jung, H.-T. Kim, and K.-T. Kim, "Construction of training database based on high frequency RCS prediction methods for ATR," *Journal of Electromagnetic Waves and Applications*, Vol. 22, Nos. 5–6, 693–703, 2008.
7. Park, S.-H., M.-G. Joo, and K.-T. Kim, "Construction of ISAR training database for automatic target recognition," *Journal of Electromagnetic Waves and Applications*, Vol. 25, Nos. 11–12, 1493–1503, 2011.

8. Toumi, A., A. Khenchaf, and B. Hoeltzener, "A retrieval system from inverse synthetic aperture radar images and its application to radar target recognition," *ELSEVIER, Information Sciences, International Journal of Informatics and Computer Science Intelligent Systems Applications*, Vol. 196, 73–96, 2012.
9. Zyweck, A., *Preprocessing Issues in High Resolution Radar Target Classification*, The University of Adelaide, Mar. 1995.
10. Mahafza, B., *MATLAB Simulations for Radar Systems Design Using MATLAB*, Chapter 7, Champman & Hall/CRC Press LLC, Jan. 2000.
11. Li, X., G. Liu, and J. Ni, "Autofocusing of ISAR images based on entropy minimization," *IEEE Trans. Aerosp. Electron. Syst.*, Vol. 35, No. 4, 1240–1251, Oct. 1999.
12. Park, S.-H., H.-T. Kim, and K.-T. Kim, "Enhanced range alignment using a combination of a polynomial and Gaussian basis functions," *Progress In Electromagnetics Research*, Vol. 95, 381–396, 2009.
13. Kim, K.-T. and H.-R. Jeong, "Identification of multi-aspect radar signals based on the feature space trajectory concept," *IEEE Trans. Ant. Propagat.*, Vol. 53, No. 11, 3811–3821, Nov. 2005.
14. Luo, S. and S. Li, "Automatic target recognition of radar HRRP based on high order central moments features", *Journal of Electronics (China)*, Vol. 26, No. 2, 184–190, Mar. 2009.
15. Park, S.-H., J.-H. Lee, and K.-T. Kim, "Performance analysis of the scenario-based construction method for real target ISAR recognition," *Progress In Electromagnetics Research*, Vol. 128, 137–151, 2012
16. Duda, R. O., P. E. Hart, and D. G. Stork, *Pattern Classification*, 2nd Edition, Wiley, New York, 2001.
17. Jdey I., et al., "Fuzzy fusion system for radar target recognition," *International Journal of Computer Applications and Information Technology*, Vol. 1, No. 3, Nov. 2012.